



PROJECT NUMBER: 101018756

ACRONYM: GTCLC-NEG

PROJECT TITLE: Development of an innovative Gas Turbine Chemical Looping Combustor for Carbon Negative Power Generation

DELIVERABLE TITLE: Particle Model

DELIVERABLE NUMBER: d3.1

Lead Beneficiary: CSIC

Work Package: WP3

Dissemination level: Public

Type: Report

Due date: 1 May 2022

Submission date: 1 May 2022

Authors: Dr. Pietro Bartocci, Dr. Alberto Abad, Dr. Arturo Cabello, Dr. Margarita de Las Obras Loscertales, Dr. Francisco Garcia Labiano

INDEX

| | |
|--|----|
| SECTION 1: PARTICLE MODELING IN PRESSURISED CHEMICAL LOOPING | 3 |
| SECTION 2: EXPERIMENTAL CAMPAIGN | 5 |
| SECTION 3: RESULTS | 8 |
| SECTION 4: BIBLIOGRAPHY | 12 |

SECTION 1: PARTICLE MODELING IN PRESSURISED CHEMICAL LOOPING

The particle modeling of the oxygen carriers produced and characterized in WP 1 is based on two publications realized at the Instituto de Carboquímica, CSIC, see [1, 2]. These works are based also on the theory developed by Levenspiel [3] when speaking of reactions catalyzed by solids and the pore diffusion resistance combined with surface kinetics. The reaction of a solid oxygen carrier with a fuel gas, e.g., CH₄, is classified as a non-catalytic gas-solid reaction. In this case, the resistance to pore diffusion is not relevant, and chemical reaction on the gas-solid interphase is the limiting step of the reaction. The kinetic model assumes that the particle is composed by small grains of the active phase, which may be spherical or have a plate-like geometry; see Figure 1. In both cases, the reaction progress following a shrinking core model.

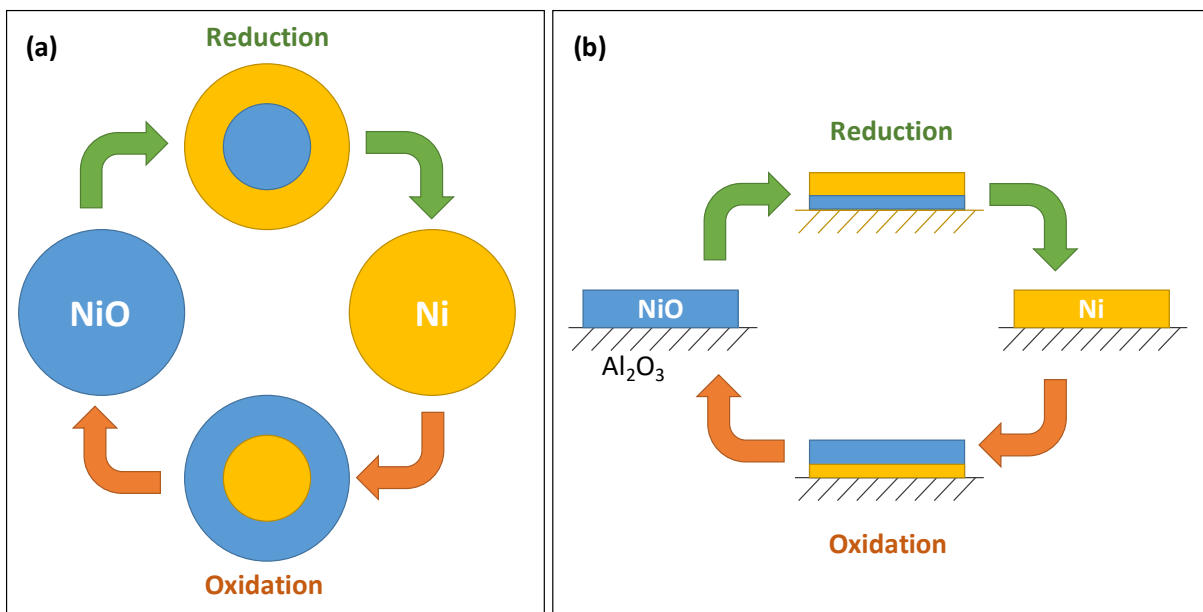


Figure 1: spherical (a) and plate-like (b) geometries for the active phase in the oxygen carrier particles.

In this project, we focused the particle model on the most interesting oxygen carrier that we have tested, which is Ni₁₈αAl. This material was prepared by impregnating nickel on porous alumina particles. The preparation method caused that the active phase (NiO) was deposited in

a thin layer on the porous structure of alumina. Therefore, NiO grains are recognized to have a plate like geometry. For this kind of geometry, the governing equations for the particle model reaction based on the Shrinking Core Model (SCM) are as follows:

$$X_r = \frac{1}{\tau^*} t \quad (1)$$

$$\tau = \frac{\tau^*}{0.8^{1/3}} \quad (2)$$

$$\frac{dX_r}{dt} = \frac{1}{\tau} \quad (3)$$

$$\tau = \frac{1}{k_r C_g^n} \quad (4)$$

$$k_r = k_{r,0} e^{-E_a/RT} \quad (5)$$

where:

- t is time (s)
- X_r is the solid conversion
- τ^* is the time for complete solid conversion in the current experiment, with the fraction of Ni as NiO being 0.8 (s)
- τ is the time for complete solid conversion assuming all Ni was as NiO (s)
- C_g is the partial pressure of the reacting gas, CH₄ in this case (mol/m³)
- n is the reaction order (-)
- k_r is the kinetic constant (m³ⁿmol⁻ⁿs⁻¹)
- $k_{r,0}$ is the pre-exponential factor of the kinetic constant (m³ⁿmol⁻ⁿs⁻¹)
- E_a is the activation energy (J/mol)
- R_g is the ideal gas constant (=8.314 J mol⁻¹ K⁻¹)

The kinetic parameters were derived through experimental tests in a pressurized thermogravimetric analyzer (PTGA) at the laboratories of Instituto de Carboquímica, ICB-CSIC.

In particular, we consider the R_o of NiO (oxygen transport capacity of nickel oxide), the nickel oxide content in the oxygen carrier (x_{NiO}), and the oxygen transport capacity of the material (R_{oc}), which is derived by multiplying the oxygen transport capacity of nickel oxide for the content of nickel oxide in the oxygen carrier. In this case:

$$R_{oc} = x_{NiO} * R_o = 0.18 * 0.2 = 0.036 \quad (6)$$

Thus, the oxygen carrier conversion may be calculated based on the mass of the sample (m) and the maximum mass variation, which is calculated by multiplying the mass of the oxidized sample (m_{ox}) by the oxygen transport capacity of the oxygen carrier (R_{oc}).

$$X_r = \frac{m_{ox} - m}{R_{oc} m_{ox}} \quad (7)$$

SECTION 2: EXPERIMENTAL CAMPAIGN

In this work, the effect of reacting pressure on the reaction kinetics will be determined in a PTGA. First, a calibration test was performed to evaluate the effect of the total pressure on the reacting conditions in the PTGA. Figure 2 shows several calibration tests using the calcium oxalate method. It was observed that the registered temperature in the 400-600 °C interval was affected by the total pressure. Thus, the reacting temperature was corrected in this interval as Table 1 shows.

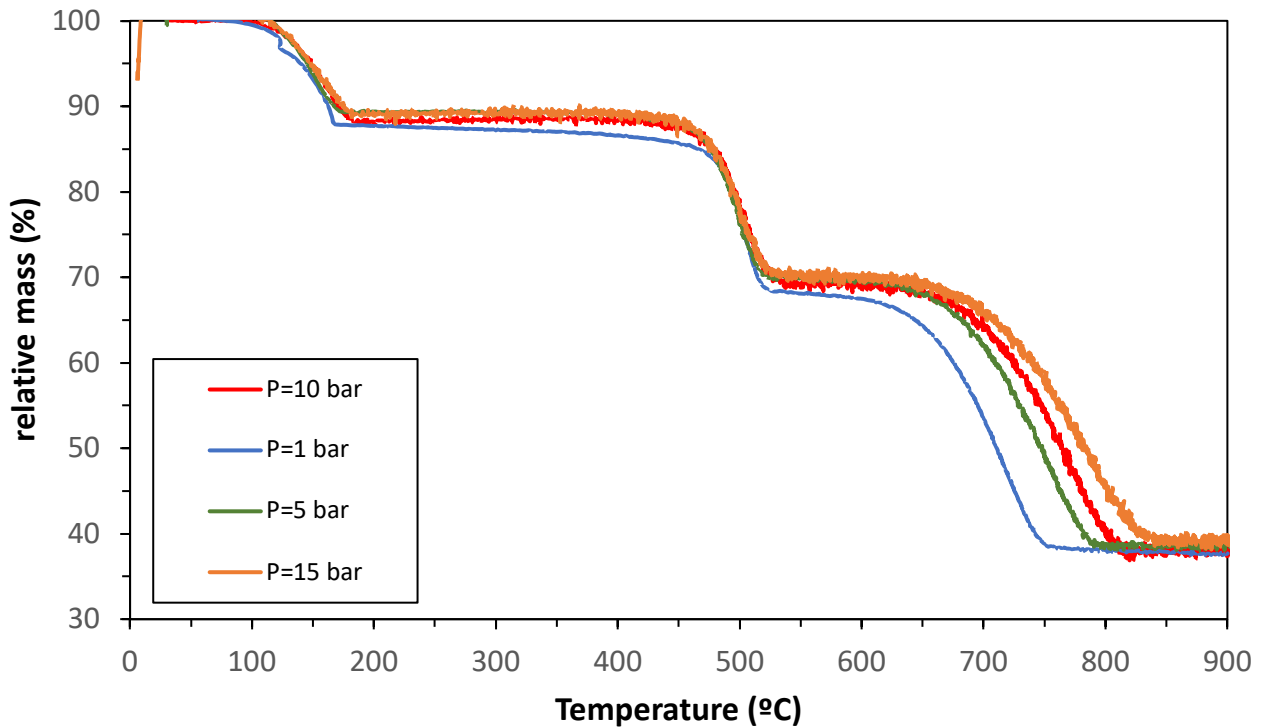


Figure 2: Calcium oxalate decomposition at different total pressure values in the PTGA.

Table 1: Adjusted temperature in the PTGA (in the range of 400-600°C)

| | |
|--------|-------|
| 15 bar | -18°C |
| 10 bar | 0°C |
| 5 bar | +6°C |
| 1 bar | +31°C |

Preliminary tests were performed by varying the mass sample or the gas flow to evaluate the effect of diffusional effects on the observable reaction rate. Then, tests at different reacting temperature, total pressure and CH₄ partial pressure values were performed using the Ni18αAl as the oxygen carrier. The tests performed are reported in Table 2. Note that when the total pressure was varied, two different series were carried out: first varying the CH₄ concentration in order to maintain constant the CH₄ partial pressure; and second, with a constant CH₄ concentration, but in this case the CH₄ partial pressure varied with the total pressure.

Table 2: Experimental campaign performed at the PTGA

| Qt (l/h) | m (mg) | T(°C) | Pt (atm) | %CH4 | %CO2 | %N2 | Air | PCH4 |
|----------|--------|-------|----------|------|------|-----|-----|------|
| 240 | 30 | 475 | 10 | 3 | 19 | 78 | 100 | 0.3 |
| 240 | 50 | 475 | 10 | 3 | 19 | 78 | 100 | 0.3 |
| 240 | 70 | 475 | 10 | 3 | 19 | 78 | 100 | 0.3 |
| 240 | 50 | 475 | 10 | 3 | 19 | 78 | 100 | 0.3 |
| 200 | 50 | 475 | 10 | 3 | 19 | 78 | 100 | 0.3 |
| 175 | 50 | 475 | 10 | 3 | 19 | 78 | 100 | 0.3 |
| 240 | 50 | 500 | 10 | 3 | 19 | 78 | 100 | 0.3 |
| 240 | 50 | 475 | 10 | 3 | 19 | 78 | 100 | 0.3 |
| 240 | 50 | 450 | 10 | 3 | 19 | 78 | 100 | 0.3 |
| 240 | 50 | 425 | 10 | 3 | 19 | 78 | 100 | 0.3 |
| 240 | 50 | 475 | 1 | 30 | 19 | 51 | 100 | 0.3 |
| 240 | 50 | 475 | 5 | 6 | 19 | 75 | 100 | 0.3 |
| 240 | 50 | 475 | 10 | 3 | 19 | 78 | 100 | 0.3 |
| 240 | 50 | 475 | 15 | 2 | 19 | 79 | 100 | 0.3 |
| 240 | 50 | 475 | 1 | 3 | 19 | 78 | 100 | 0.03 |
| 240 | 50 | 475 | 5 | 3 | 19 | 78 | 100 | 0.15 |
| 240 | 50 | 475 | 10 | 3 | 19 | 78 | 100 | 0.3 |
| 240 | 50 | 475 | 15 | 3 | 19 | 78 | 100 | 0.45 |

Figure 3 shows an example of mass variation for consecutive redox cycles varying the reacting temperature. The variation of the sample mass corresponded to the oxygen depletion during reduction or its replenishment during oxidation:

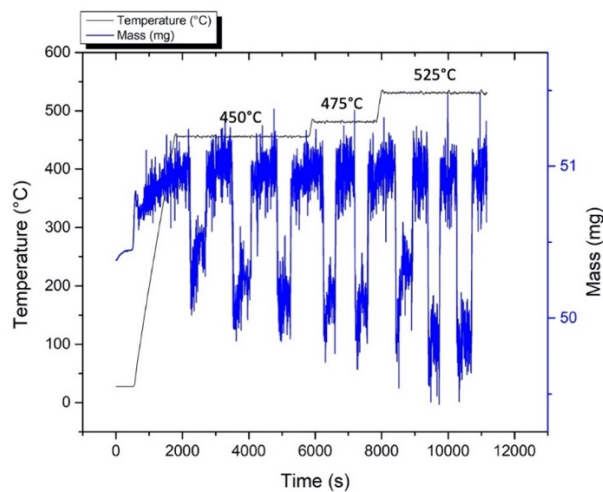
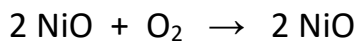


Figure 3: Mass variation for consecutive redox cycles varying the reacting temperature

SECTION 3: RESULTS

The effect of the total pressure, the partial pressure of CH₄ and the reacting temperature on the reaction kinetics of NiO reduction was determined by PTGA tests with the Ni18αAl material. Thus, the reaction order at 5 and 15 atm was determined by considering the variation of the reaction rate when the molar fraction of CH₄ was varied. Thus, the reaction order may be obtained by linearizing Eq. (4):

$$\ln(\tau) = -\ln(k_r) - n \ln(C_g) \quad (8)$$

Figure 4 shows a plot of $\ln(\tau)$ vs. $\ln(C_g)$. The slope of the linear fitting is the reaction order. It can be seen that the n value barely changed with the total pressure from 0.74 to 0.79. An average value of $n=0.76$ may be taken. The y-intercept is $\ln(k_r)$; then k_r was 0.011 and 0.0067 m^{2.28}mol^{-0.76}s⁻¹ at 5 and 15 atm, respectively.

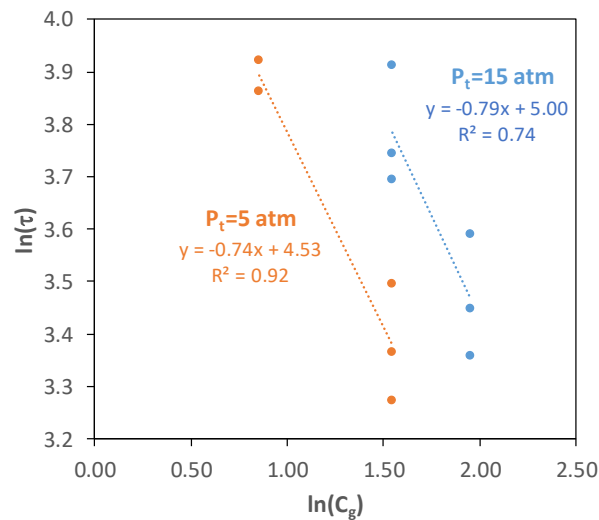


Figure 4: Effect of the CH₄ concentration, C_g, on the τ parameter at 5 and 15 atm. T = 779 K.

Therefore, the apparent kinetic constant, k_r , was affected by the total pressure. Several tests at different total pressures were performed at 779 K and 3 vol.% CH₄ in the PTGA. The determined reaction rates, dX_r/dt , decreased when the total pressure increased from 1 to 5 atm. Then, the reaction rate progressively increased with the total pressure at 10 and 15 atm; see Figure 5. This behavior was related to a decrease of the apparent

kinetic constant, k_r . Figure 4 shows the variation of k_r with the total pressure.

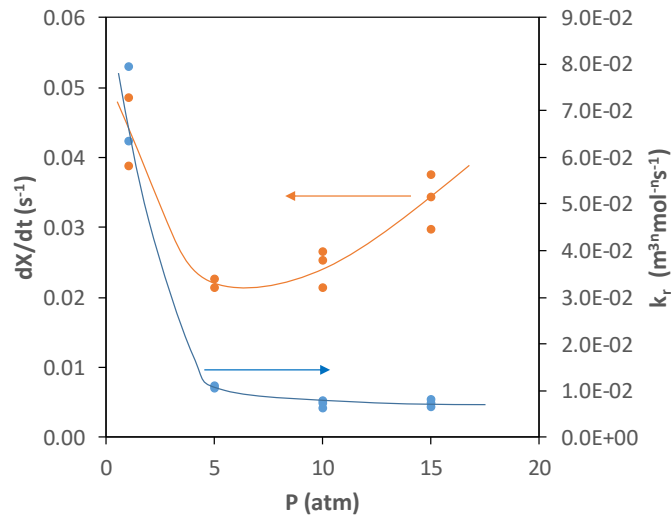


Figure 5: Variation of the reaction rate and the apparent kinetic constant with the total pressure. $T = 779 \text{ K}$.

To determine the effect of the total pressure on the apparent kinetic constant, additional tests were performed varying the total pressure but maintaining constant the CH_4 partial pressure. Figure 6 shows the evolution of the calculated apparent kinetic constant, k_r , with the total pressure. It was determined that the effect of the decrease in k_r was stronger at low total pressure, and then it was less relevant for elevated pressures. In order to predict the k_r value as a function of the total pressure, the following equation was proposed:

$$k_r(P) = \frac{k_r(P=1\text{atm})}{P_t^d} \quad (9)$$

where d is a fitting parameter to consider the effect of total pressure on the kinetic constant. From the fitting shown in Figure 6, it was determined that $d=0.9$.

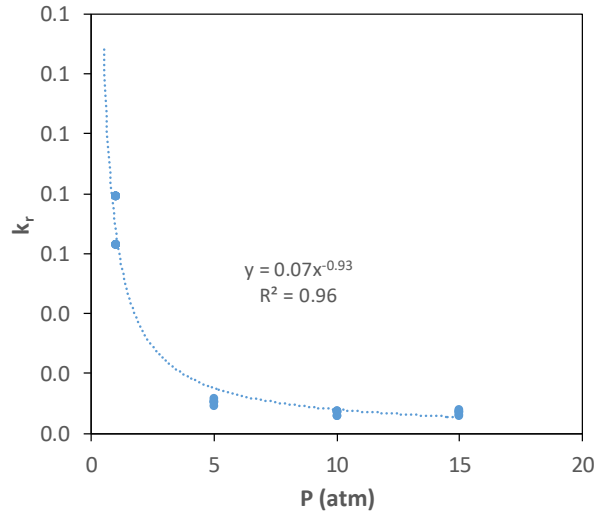


Figure 6: Effect of total pressure in the apparent kinetic constant, k_r . $T = 779$ K.

Finally, the effect of the reaction temperature on the kinetic constant was considered. Tests at 10 atm were performed at different temperatures between 729 and 804 K. Figure 7 shows that the apparent kinetic constant increased with temperature. An Arrhenius-type dependency of k_r with temperature was assumed:

$$k_r = k_{r,0} e^{-E_a/(R_g T)} \quad (10)$$

$$\ln(k_r) = \ln(k_{r,0}) - \frac{E_a}{R_g} \frac{1}{T} \quad (11)$$

Thus, the activation energy (E_a) was calculated from the slope of Figure 7, while the pre-exponential factor, $k_{r,0}$, could be calculated from the y-intercept. The calculated values for these parameters were $k_{r,0}(P=10 \text{ atm}) = 204 \text{ m}^{2.28} \text{ mol}^{-0.76} \text{ s}^{-1}$ and $E_a = 65.8 \text{ kJ/mol}$. Considering Eq. (9), may be calculated that the pre-exponential factor for 1 atm is $k_{r,0}(P=1 \text{ atm}) = 1.74 \cdot 10^3 \text{ m}^{2.28} \text{ mol}^{-0.76} \text{ s}^{-1}$.

Therefore, the following equation was derived to calculate the kinetic constant as a function of the reacting temperature and the total pressure:

$$k_r = \frac{1.74 \cdot 10^3}{P_t^{0.9}} e^{-65800/(R_g T)} \quad (12)$$

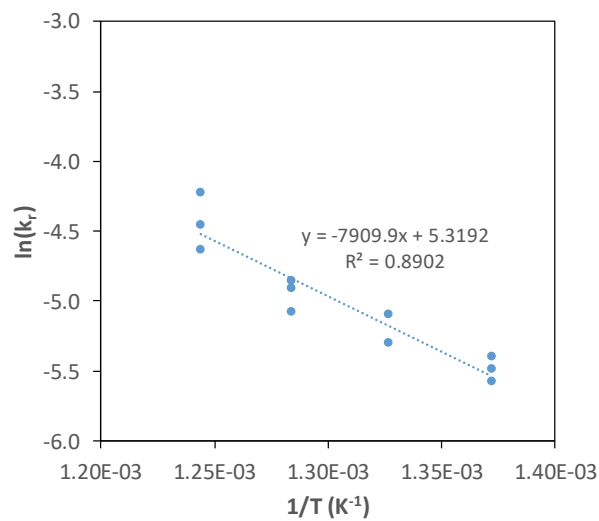


Figure 7: Effect of the reacting temperature on the kinetic constant.

Bibliography

1. Abad, A., et al., *Reduction kinetics of Cu-, Ni-, and Fe-based oxygen carriers using syngas (CO+H₂) for chemical-looping combustion*. Energy & Fuels, 2007. **21**(4): p. 1843-1853.
2. Garcia-Labiano, F., et al., *Effect of pressure on the behavior of copper-, iron-, and nickel-based oxygen carriers for chemical-looping combustion*. Energy & Fuels, 2006. **20**(1): p. 26-33.
3. Levenspiel, O., *Chemical reaction engineering*. 1998: John Wiley & Sons.
4. Gayan, P., et al., *NiO/Al₂O₃ oxygen carriers for chemical-looping combustion prepared by impregnation and deposition-precipitation methods*. Fuel, 2009. **88**(6): p. 1016-1023.